

MODELLING AND SIMULATION OF THE GASEOUS FISSION PRODUCT REMOVAL IN THE MOLTEN SALT FAST REACTOR

Federico Caruggi, Antonio Cammi, Eric Cervi, Andrea Di Ronco, Stefano Lorenzi

Department of Nuclear Engineering

Politecnico di Milano

Via la Masa 34

20156, Milan, Italy

federico.caruggi@mail.polimi.it, antonio.cammi@polimi.it; eric.cervi@polimi.it;

andrea.dironco@polimi.it; stefano.lorenzi@polimi.it

ABSTRACT

The Molten Salt Fast Reactor, currently under development in the framework of the SAMOSAFER H2020-Euratom project, foresees an in-core helium bubbling system for the removal of gaseous and metallic fission products from the fuel salt. The correct assessment of the removal capability of the off-gas system inside the fuel circuit is of paramount importance in the determination of the radioactive source term in the MSFR. This paper deals with the extension of the modelling capabilities of an OpenFOAM multiphysics solver previously developed at Politecnico di Milano and its application to study the transport of the gaseous fission products (GFPs). In particular, the behavior of GFPs and their interaction with the MSFR helium bubbling system are considered to determine the mass transfer of GFPs from the salt mixture to the gaseous phase and then to the off-gas system. xenon-135 is taken as the reference isotope for modelling the production, the transfer between liquid and gaseous phases (i.e. the fuel salt and helium, respectively), and the extraction of the gases. The capabilities of the solver are presented with an analysis carried out on a simplified axisymmetric model of the reactor. The efficiency of the helium bubbling system in the removal of the gaseous fission products is evaluated through a characteristic renewal time of the core calculated from the outcomes of the simulation. The latter is found to be in the order of tenths of seconds in accordance to preliminary assessments performed by reactor designers.

KEYWORDS

Multiphysics, OpenFOAM, Molten Salt Fast Reactor (MSFR), Gaseous Fission Products (GFP), Helium bubbling

1. INTRODUCTION

The Molten Salt Fast Reactor (MSFR) is the reference design for the development of Molten Salt Reactors in the framework of the Generation IV International Forum (GIF-IV) [1]. It is a circulating-fuel reactor, featuring a mixture of fluoride salts acting both as fuel and coolant and employing a Thorium fuel cycle [2]. The design presents various innovative characteristics with respect to conventional nuclear systems, offering potential advantages, particularly in terms of economy and safety. The presence of new features, however, implies the need to create and develop new computational tools, suitable for their modelling and simulation. One particular characteristic of the design is the foreseen presence of a in-core helium bubbling system, envisaged for a better removal of gaseous and metallic fission products from the fuel [3].

In past works, a multiphysics solver for the analysis of the MSFR was developed in the framework of OpenFOAM [4]. The multiphysics approach was chosen in view of the particularly strong coupling between thermo-hydraulics and neutronics in this kind of nuclear systems. The solver is based on the Euler-Euler

formulation to model the presence of two phases - a liquid one for the salt and a gaseous one for helium bubbles - and their interactions, considering also neutronics and the transport of delayed neutron and decay heat precursors.

Knowledge of the spatial distribution of the fission products inside the core is a fundamental information for a circulating-fuel reactor, since they influence heavily the neutronics of the system and their contribution is crucial in the estimation of the source term, both inside and outside of the core. Additionally, an accurate study on the effect of the helium bubbling system is required in order to understand if it is a viable option for the removal of fission products. In the past, the impact of the helium bubbles has been modelled in analogy with a radioactive decay of the interested nuclides, with the definition of a characteristic time, employing a value of 30 seconds [5]. The aim of this paper is to introduce in the multiphysics environment the capability of modelling the gaseous fission products in the reactor, considering their production and consumption and, most importantly, their interactions with the helium bubbling system. This allows for the calculation of a characteristic time, able to express the efficiency of the bubbles in the removal of the gaseous fission products. In addition, it makes possible to verify the reliability of the assumptions made in the past and to take into account 3D effects in the fission product removal.

The paper is organized as follows. The new sub-model for the fission product modelling is described in Section 2. In Section 3, simulations are performed on a 2D model of the MSFR system in order to test the new capabilities and to perform the necessary analyses on the behavior of gaseous fission products and the helium bubbling system. Finally, in Section 4, some conclusions are drawn.

2. XENON MODELLING

In this work, Xe-135 is taken as a reference nuclide for the analysis of all those fission products that are generated as solute in the fuel and that can be extracted and carried to the off-gas system by the action of the helium bubbling system. In the remainder of this Section, all the assumptions made in the development of this feature are presented and discussed, both from the physical and the implementation points of view.

2.1. Theoretical Approach

The starting point of this work, as aforementioned, is a previously developed Euler-Euler multiphysics solver, able to model both the thermal-hydraulic and neutronic aspects of the MSFR, considering the presence of the helium bubbles in the core [4,6]. In order to adapt it to the presence of xenon and other GFPs, the algorithm was modified with the definition of multiple species for each phase (salt and xenon in the liquid, xenon and helium in the gaseous one). This choice of approach in particular gives the possibility to model the production of xenon directly in the salt, with a dependence on the neutronics of the system, together with the ability to simulate the foreseen migration to the gas bubbles through suitable mass transfer models, and the consequent transport out of the core towards the off-gas system.

In order to model the presence of multiple species in each phase, suitable equations are added in the solver algorithm, in order to describe the concentration of the components in terms of production, transport and consumption. A general formulation for species i in phase k as follows

$$\frac{\partial \alpha_k C_{i,k}}{\partial t} + \nabla \cdot (\alpha_k \mathbf{u}_k C_{i,k}) - \nabla \cdot (\alpha_k D_k \nabla (C_{i,k})) = \frac{dm_{i,k}}{dt} \quad (1)$$

where $C_{i,k}$ is the concentration expressed in kg/m^3 , D_k represents the mass diffusivity in the phase, and $\frac{dm_i}{dt}$ denotes the mass transfer of the species to or from the phase. The diffusivity coefficient of each phase, D_k , can be calculated from the dimensionless Schmidt number, Sc , as

$$D_k = \frac{\mu_k}{\rho_k Sc_k} \quad (2)$$

The rate of mass transfer of species i in phase k can be computed through a suitable coefficient, $K_{i,k}$:

$$\frac{dm_{i,k}}{dt} = K_{i,k} a_i (C_{i,k}^* - C_{i,k}) \quad (3)$$

where C^* denotes the saturation concentration at the interface, and a represents the interfacial area of exchange per unit volume (of system geometry), which is dependent on the pair of phases where the component is present. In our particular case, for a liquid-gas system, this term is computed from the bubble diameter (d_b) as

$$a_{l/g} = \frac{6 \alpha_g}{d_b} \quad (4)$$

At this point, in order to solve the species transport equations, there is the need to obtain the mass transfer coefficient and the saturation concentration of Eq. 3 for each component in each phase. This can be done exploiting, respectively, a mass transfer model and an interface composition one. For what concerns the interface composition model, an Henry-like behavior is chosen. The saturation concentration at the interface for one phase is thus computed from the concentration of the specie on the other phase as

$$C_{i,k}^* = H C_{i,j} \quad (5)$$

where H is the dimensionless Henry coefficient.

The mass transfer model aims at computing the term K in Eq. 3. Since the diffusivity in each phase is already part of the solution, this is generally done exploiting the definition of a dimensionless group, the Sherwood number, representing the ratio between convective and diffusive mass transfer

$$K_{i,k} = \frac{Sh D_{i,k}}{d_b} \quad (6)$$

The Sherwood number is generally evaluated through empirical correlations, depending on the particular conditions of the flow in the case of interest. These models can be derived from both analytical and experimental studies and, for the case of gaseous bubbles in liquid flows, they generally result in an analogy with the heat transfer correlations (Dittus-Boelter-like laws, where Nu and Pr are replaced respectively by Sh and Sc):

$$Sh = A Re_b^B Sc^C \quad (7)$$

It is worth noting that the Reynolds number employed in these formulation is the one referring to a single bubble transported by the liquid. In this formulation, the characteristic length is the diameter of the bubble (calculated, in this work, as a function of pressure), and the velocity is the difference between that of the bubble and the one of the liquid some distance away (so that the value is not influenced by the presence of the bubble itself) [7]:

$$Re_b = \frac{|\mathbf{u}_g - \mathbf{u}_l| d_b}{\nu_l} \quad (8)$$

Among the various correlations taken into account, the one proposed by Higbie [8] could be exploited for the MSFR system:

$$Sh = 1.13 Re^{1/2} Sc^{1/2} \quad (9)$$

This particular formulation has been developed for the case of free-rise of bubbles in a liquid stream, which is a condition somewhat similar to the MSFR environment. The main limitation is that this approach refers to a laminar stream, while the regime of flow for the MSFR is expected to be turbulent. Given the lack of experimental data, however, the approximation can be considered acceptable.

2.2. Code Implementation

In the OpenFOAM environment, to deal with multiple components in each phase, the algorithm calls for the solution of species transport equations, based on Eq. 1. Since the solver is developed for the treatment of compressible flow, however, a concentration depending on the volume is not suitable. The problem is avoided in OpenFOAM by making use of a different expression, employing the mass fraction of the component in the phase (with units of kg/kg),

$$Y_{i,k} = \frac{C_{i,k}}{\rho_k} \quad (10)$$

The formulation of the species transport equation treated by the solver is thus [9] [10]

$$\frac{\partial \alpha_k \rho_k Y_{i,k}}{\partial t} + \nabla \cdot (\alpha_k \rho_k \mathbf{u}_k Y_{i,k}) - \nabla \cdot \left(\frac{\alpha_k \mu_k}{Sc_k} \nabla (Y_{i,k}) \right) = \frac{dm_{i,k}}{dt} \quad (11)$$

The algorithm builds a similar equation for each component in each phase. In order to properly simulate the behavior of xenon in the system, some more terms need to be supplied to reproduce the production and the consumption of the fission products.

The isotope 135 of xenon is generally considered one of the most influential species in a nuclear environment, in its role as a neutronic poison. Its contribution is somewhat limited in a fast reactor as the MSFR, but the presence of data related to its behavior in a thermal system can be employed as a solid starting point. Additionally, the analyses conducted here can be easily extended to any other nuclide of higher relevance identified in the future. In a reactor Xe-135 is produced both as a direct fission product (with a certain yield), and as result of the decay of other fission products, I-135 and Te-135, which are precursors in its decay chain. A complete formulation of the problem would require the solution of a balance equation for each one of these nuclides but, as a first approximation, it is possible to consider only the presence of Xe, as if it was produced all by fission, with an equivalent cumulative yield. A source term is thus inserted in the transport equation relative to the liquid phase, in a form of direct proportionality with the fission rate of the system

$$S_{Xe} = y_{Xe} \frac{m_{mol}}{N_{Av}} \sum_n (\Sigma_{f,n} \varphi_n) \quad (12)$$

where m_{mol} is the molar mass of Xe-135 and N_{Av} is the Avogadro number.

Together with the source term, some sink terms need to be introduced in the equations as well. Apart from manual removal of the gaseous phase, neutron are subject to capture and decay. Again, for the sake of simplicity, only Xe-135 is considered and the rest of the decay chain is neglected. The component is thus modelled as if disappearing after both capture and decay.

$$\text{sinks} = -\alpha_k \rho_k \left(\lambda + \sum_n (\sigma_{c,n} \varphi_n) \right) Y_{Xe,k} \quad (13)$$

The capture cross sections are evaluated by means of a Monte Carlo code for burnup and transport calculations, Serpent-2 [11].

The final forms of the xenon balance equations as implemented in OpenFOAM are, for liquid and gas phase respectively,

$$\frac{\partial \alpha_l \rho_l Y_{Xe,l}}{\partial t} + \nabla \cdot (\alpha_l \rho_l \mathbf{u}_l Y_{Xe,l}) - \nabla \cdot \left(\frac{\alpha_l \mu_l}{Sc_l} \nabla (Y_{Xe,l}) \right) = S_{Xe} - \alpha_l \rho_l \left(\lambda + \sum_n (\sigma_{c,n} \varphi_n) \right) Y_{Xe,l} + \frac{dm_{Xe,l}}{dt} \quad (14)$$

$$\frac{\partial \alpha_g \rho_g Y_{Xe,g}}{\partial t} + \nabla \cdot (\alpha_g \rho_g \mathbf{u}_g Y_{Xe,g}) - \nabla \cdot \left(\frac{\alpha_g \mu_g}{Sc_g} \nabla (Y_{Xe,g}) \right) = -\alpha_g \rho_g \lambda Y_{Xe,g} + \frac{dm_{Xe,g}}{dt} \quad (15)$$

$$S_{Xe} = y_{Xe} \frac{m_{mol}}{N_{Av}} \sum_n (\Sigma_{f,n} \varphi_n) \quad (16)$$

$$\frac{dm_{Xe,l}}{dt} = -\frac{dm_{Xe,g}}{dt} = \frac{6 \alpha_g Sh}{d_b^2} D_{Xe,l} \rho_l \left(HY_{Xe,g} \frac{\rho_g}{\rho_l} - Y_{Xe,l} \right) \quad (17)$$

Neutronics is solved following the multigroup diffusion approach, employing in particular a power iteration routine to achieve critical conditions. This means that the transient of the neutronic quantities caused by the injection of helium was neglected. Six-groups constant are generated with the Serpent-2 code, employing the cross section from JEFF-3.1.1 libraries [12]. Albedo boundary conditions are defined both at the reflectors and the blanket walls, with Eq. 18.

$$D_{n,i} \nabla \varphi_i = -\frac{1}{2} \left(\frac{1 - \beta_i}{1 + \beta_i} \right) \varphi_i \quad (18)$$

The neutronic part of the algorithm is also capable to solve for the transport of delayed neutron precursors as well as decay heat precursors, for which suitable multi-groups models are defined, taking into account also the turbulence aspects of the problem. More details on the neutronic approaches employed can be found in [4] and [6].

3. REACTOR ANALYSIS

The modelling approach described earlier allows for the simulation, in the OpenFOAM environment, of the behavior of gaseous fission products in the MSFR system. In the following, this tool is exploited for the analysis of the effect of the helium bubbling system on the concentration of these species. Since the apparatus is envisaged for a faster and more controlled removal of the non-soluble (gaseous and metallic) components of the mixture, the calculation of a removal rate and a characteristic time is performed on the reference nuclide Xe-135, in order to assess the efficiency of the helium bubbles in their foreseen task.

3.1. Geometry

For these analyses, a simplified reactor geometry is adopted. The basis for this choice is taken from the work of the past EVOL project [13]. In particular, a 2D axisymmetric model is employed, so that the cylindrical symmetry can be exploited in the solution of the problem. Only the fluid part of the system (salt and helium bubbles) is taken into account, in order to avoid the increased computational effort that modelling the solid parts as well would require. A sketch of the geometry employed, with indications relative to the helium bubbling system, the heat exchanger and the pump location, is shown in Fig. 1a. The latter are modelled by means of a convective heat condition and a momentum source, respectively, uniformly distributed in the

corresponding sections. Finally, a free surface is present in the upper right corner of the hot leg, in order to allow for the expansion of the mixture. Fig. 1b represents the computational mesh applied to the geometrical domain to perform the simulations, consisting of 22671 elements in total.

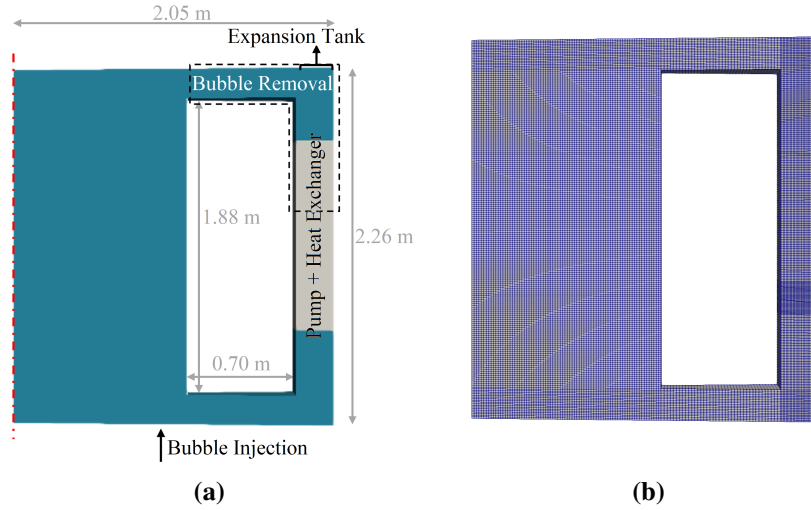


Figure 1. (a) Geometry and (b) Computational mesh employed for 2D simulations

3.2. Efficiency of the Bubbling System on Xenon

The effectiveness of the helium bubbles in the removal of the gaseous fission products is analyzed in this work by defining and computing a suitable parameter, in the simulation of the behavior of the reference isotope xenon-135, i.e. a characteristic renewal time which is connected to the cycle time of the removal process. A fundamental hypothesis is made in this instance, assuming that the effect of the bubbling system on the mass balance of the gaseous fission products can be modelled in perfect analogy with a radioactive decay, upon definition of a corresponding constant parameter, γ_{bub} . From an analytical point of view, this is represented by a linear sink term in the differential equation relative to the balance of the nuclide, for which a simplified version can be written as:

$$\frac{\partial N}{\partial t} = source - reactions - \lambda_{dec}N - \gamma_{bub}N \quad (19)$$

This approach is already employed in the burnup analysis of the MSFR, in the solution of the Bateman equations. There, to correctly predict the evolution of the salt mixture, it is of paramount importance to take into account the effects related to the FP removal, from both the gaseous system and the fuel treatment unit [14]. The added contribution translates, upon integration, in an exponential trend in time for the mass balance of the interested nuclide, in analogy with the radioactive decay. The helium bubbling system can be considered effective in the removal of the gaseous fission products, then, if its impact is enough to drive the dynamics of the nuclide concentration. This means, from the analytical point of view, that the related parameter γ_{bub} is considerably larger than both the decay constant of the nuclide and the characteristic parameters of the nuclear reactions involved (products of neutronic flux and proper cross sections), or alternatively that the characteristic time of the removal via bubbling is small with respect to the others. The nominal value of 30 seconds used in the past by MSFR designers is surely small enough to meet this criterion, but there is still the need to confirm the assumption on a realistic case of study. Part of the aim of this work is thus to verify

if it is possible to obtain results in the same order of magnitude with a CFD simulation, able to take into account the real bubble distribution and the phenomenon of mass exchange.

Following the approach just depicted, the necessary parameter is directly calculated as the ratio between the rate of extraction of xenon from the system via bubbling and the integrated mass inventory present in the system itself:

$$\frac{Xe_{outflow} (kg/s)}{Xe_{mass} (kg)} = \frac{\gamma_{bub} Xe_{mass}}{Xe_{mass}} = \gamma_{bub} (1/s) \quad (20)$$

The cycle time of the removal process mentioned above is nothing else than the reciprocal of this coefficient:

$$\tau = \frac{1}{\gamma_{bub}} \quad (21)$$

The mass inventory of xenon in the system is calculated as a numerical output of the simulations, by integrating the concentration on the domain. The removal of the gaseous phase from the system is modeled by the introduction of an implicit mass sink term in the continuity equation. This approach allows to reproduce a continuous extraction of gas, distributed over a chosen section of the volume, by an amount which is proportional to the quantity present in the system. In particular, for this work, the action of the remover is confined to the hot leg of the reactor. The effect produced is sufficient to extract all the gas located in the external circuit, so that there are no bubbles re-entering the core from the cold leg via recirculation. This means that all the mass of xenon present in the gaseous flow going out of the core is effectively removed from the system, together with the additional quantity migrating to the gaseous phase in the hot leg. The rate of removal from the system can be obtained with a direct calculation from the values of mass inventory in the domain, recorded for consequent time intervals, with an added term to account for the continuous production of xenon (which is given by Eq. 12):

$$Xe_{outflow}(t) = -\frac{Xe_{mass}(t) - Xe_{mass}(t - \Delta t)}{\Delta t} + S_{Xe} \quad (22)$$

3.3. Simulations and Results

The simulations were performed, as already mentioned, on an axisymmetric 2D model. The stationary conditions are found initially in the presence of the single phase only. The quantities of main importance in the core are displayed, in form of color map plots, in Fig. 2. As it can be seen, the simplified geometry suffers from the arising of a stagnation zone, where xenon is accumulated, caused by the presence of straight walls and squared angles. This factor can be of particular influence in the removal of the gaseous fission products, if the bubbles are unable to reach the whole available core space, especially for those species for which the diffusivity in the salt is low.

The steady state conditions found are taken as starting point for the two-phase simulations. The injection and extraction of gaseous phase are modelled following the indications of Figure 1a. For the velocity fields, no-slip boundary conditions are employed at the reactor walls, and atmospheric pressure is imposed at the free surface of the expansion tank. The standard k- ϵ model is employed to account for turbulence of the fuel. The diameter of the helium bubbles is estimated by use of an isothermal power law, dependent on pressure:

$$d_b = d_0 \left(\frac{p_0}{p} \right)^{1/3} \quad (23)$$

where the reference diameter and pressure are assumed to be, respectively, $d_0 = 3$ mm, $p_0 = 1$ atm.

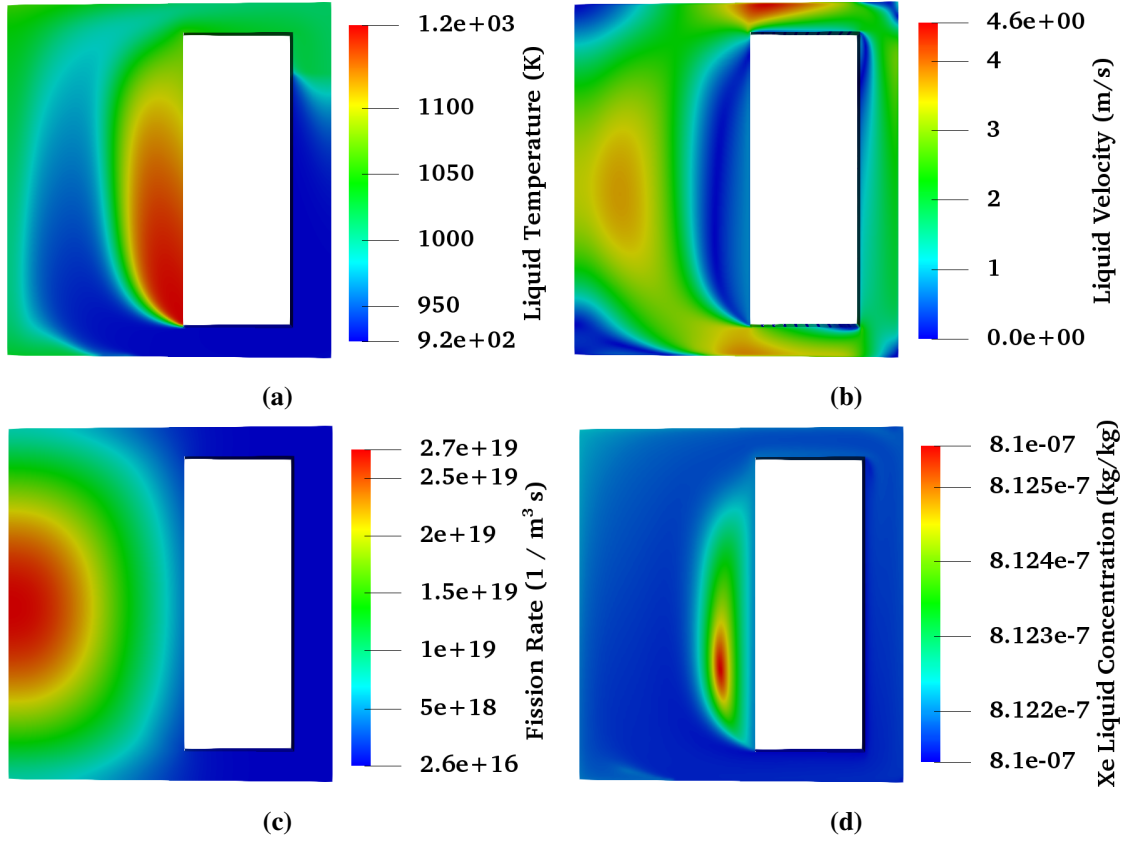


Figure 2. Color map plots for the profiles of the main quantities in 2D simulations. (a) Temperature (b) Velocity (c) Fission Rate (d) Xe concentration

The explicit terms in the momentum balance equation, for the interactions between the phases, are treated with the following correlations:

- For virtual mass forces, a constant coefficient correlation is chosen, with $C_{VM} = 0.5$ [15]
- Lift is not considered, following the assumption that the bubbles are sufficiently small in size to neglect the effect of vorticity on the momentum transfer between the two phases
- Turbulent dispersion is neglected as well
- The drag coefficient is evaluated by use of the Schiller-Naumann correlation [16], which depends on the bubble Reynolds number defined in Eq. 8:

$$C_D = \begin{cases} \frac{24(1+0.15Re_b^{0.687})}{Re_b} & \text{for } Re_b < 1000 \\ 44 & \text{for } Re_b \geq 1000 \end{cases} \quad (24)$$

The heat transfer between the phases is modelled following the Ranz-Marshall correlation [17]:

$$Nu = 2 + 0.6 Re_b^{1/2} Pr^{1/3} \quad (25)$$

All of the modelling assumptions just mentioned follow same approach chosen in previous works conducted with the same solver. In particular, in Chapter 3 of [18], a sensitivity analysis is proposed, putting in evidence the suitability of the correlations used.

Mass transfer between the liquid phase and the dispersed bubbles is modelled with Henry's law, and the Sherwood number is evaluated through the Higbie correlation (Eq. 9), as mentioned in Section 2.

The transport of the gaseous bubbles alone develops in short time, and the phase fraction reaches, for the reference case, the steady-state distribution shown in Fig. 3. As it can be seen, helium bubbles are injected from the bottom of the core, with null velocity, and they are carried by the fuel to the cold leg up top, where they are progressively removed from the system. During this transit, xenon is extracted from the liquid phase through mass transfer, and it is carried away by the helium flow. The overall effect on the concentration of Xe-135 can be modelled, as mentioned, in analogy with a radioactive decay, with the calculation of a removal constant, and a corresponding renewal time. Fig. 4 displays the resulting distribution of xenon concentration in the salt at the end time (100 seconds) of the reference simulation. The reduction of inventory is quite evident with respect to the results shown in Fig. 2d, leading to a decrease by a factor of approximately 2.3. On the other hand, it should be pointed out that this is not the equilibrium profile for the concentration in presence of the bubbling flow, and the simulation time needed to reach the steady-state conditions for the transport and removal of the xenon component is much longer.

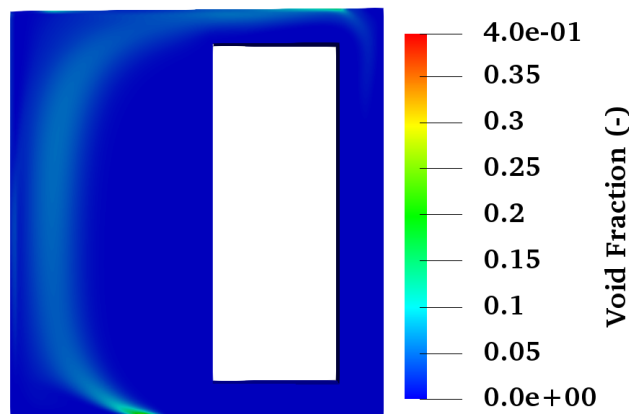


Figure 3. Void fraction profile for the reference case

The main figure of merit obtained from the 2D simulations is the characteristic time defined by Eq. 21. The graph in Fig. 5 represents its behavior in time for the reference case. As it can be seen, after a first steep transient, the curve acquires a flat profile, and the parameter reaches a steady-state value which remains almost constant from there on, even if the stationary conditions are not met yet at the end of the simulation. The reference conditions chosen for the helium bubbling system modelling are portrayed in the Figure as well.

The flat profile that the curve just displayed assumes after the initial transient can be seen as a hint that the xenon removal through helium bubbling system acts effectively in analogy with a radioactive decay, with the selection of an appropriate time constant. As further confirmation of this fact, the graph in Fig. 6 shows the xenon inventory in the system through time. The regression of the curve puts in evidence the

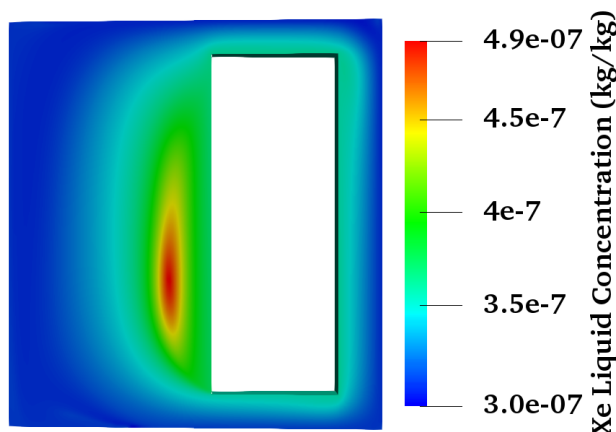


Figure 4. Xenon concentration profile at the end of the reference simulation

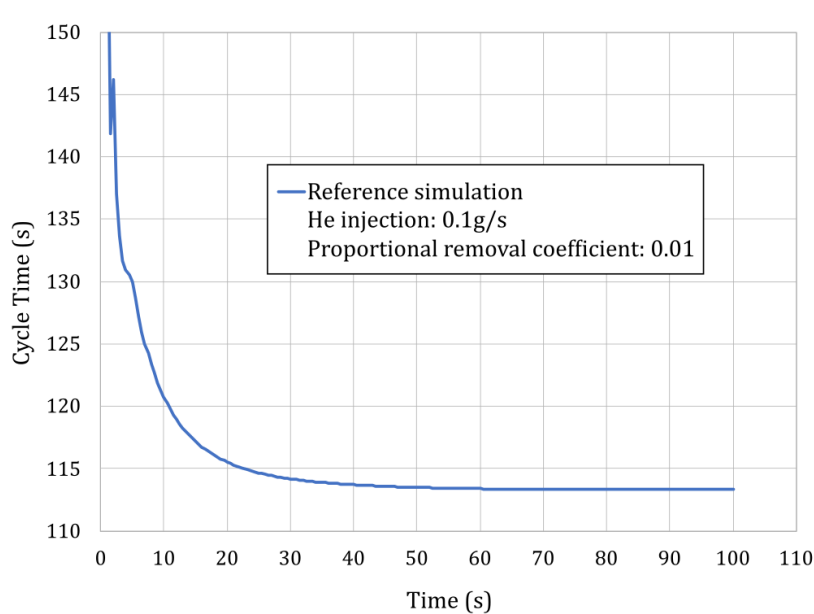


Figure 5. τ trend in time for the reference case

exponential trend associated with decay. It should be pointed out that the real behavior in time is not a simple exponential, and this regression is valid only for the initial transient, where the dynamic is driven by the effect of the remover alone. The aim of the work is, however, to estimate the removal capability of the helium bubbling system, rather than establishing the final steady-state conditions of the reactor, and the graph displayed is meant only to confirm the validity of the hypothesis made in the modelling of the effect of bubbles on the xenon concentration.

The result shown in Fig. 5 is obviously dependent on a series of parameters chosen to perform the reference

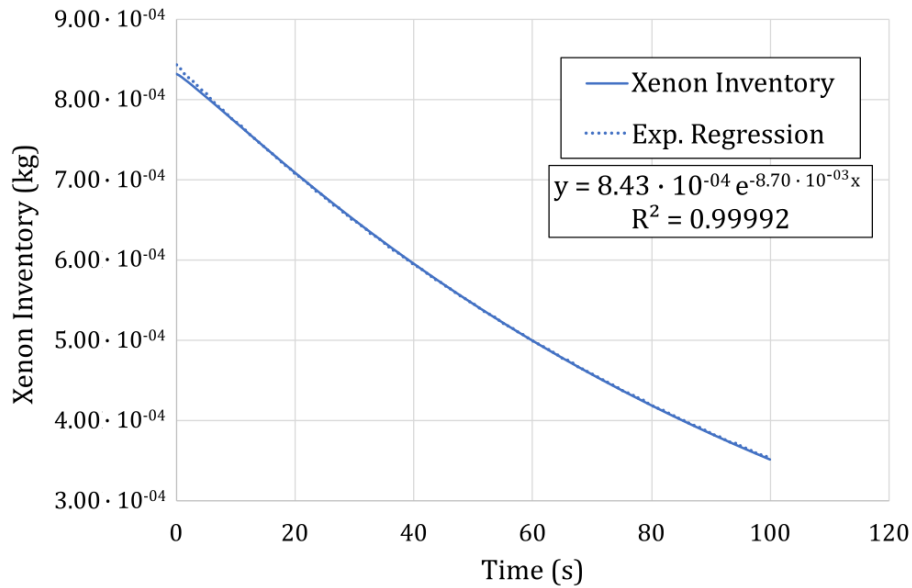


Figure 6. Xenon inventory trend in time for the reference case, with exponential regression

simulation. The main quantity of relevance in the definition of the problem is considered to be the mass flow rate of helium injected in the system. Multiple simulations were thus performed with different values for this parameter, keeping all the other conditions unaltered. The result, in terms of comparison of values for the characteristic renewal time, is presented in Fig. 7.

From the plot, it can be seen that the time needed to complete the transient and reach the steady-state value is always shorter than the one seen in the reference case (with the lowest helium inlet flow rate). Additionally, the τ shows an inversely proportional behavior with respect to the inlet mass flow rate of helium. This fact gains further confirmation by the display of Fig. 8, where the values of characteristic time are plotted in function of the parameter, for two distinct moments of time in the simulations. The proportionality trend is clearly visible, and it is numerically verified by the data in Table I.

Additionally, the results reported here show that the aforementioned value of 30 seconds supposed by the MSFR designers for the characteristic time of the gaseous fission products removal can be effectively reproduced in CFD simulations under some conditions, and the order of magnitude of the quantity is the correct one for the whole range of values of helium inlet flow rate considered.

4. CONCLUSIONS

In this paper, a previously developed multiphysics OpenFOAM solver for the analysis of the MSFR is extended, with the introduction of the capability to model the presence of gaseous fission products, for what concerns their production, consumption, motion in the salt and interactions with the helium bubbling system. The efficiency of this latter apparatus is analyzed, with the definition of a suitable parameter (the renewal time). The results, based on the simulation of the behavior of the reference nuclide Xe-135, show that the value of 30 seconds suggested theoretically by the designers is of the right order of magnitude. An

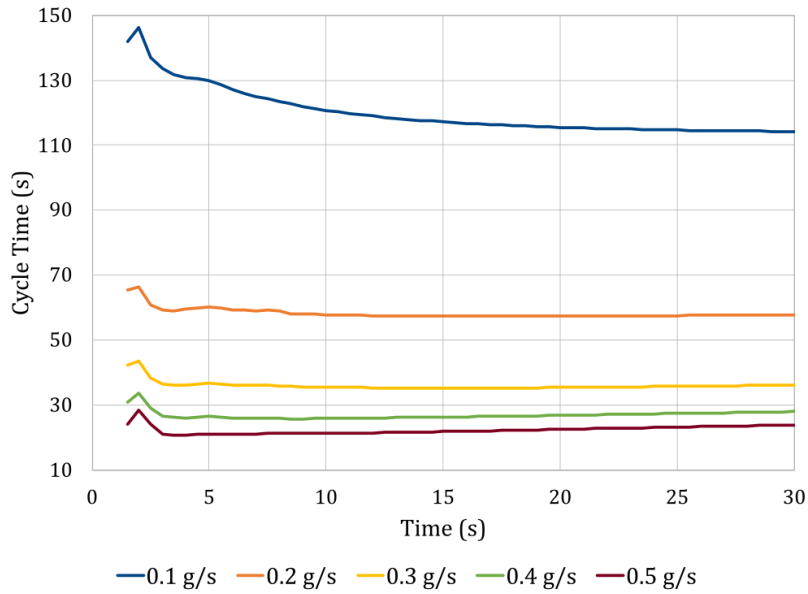


Figure 7. τ trends in time for different values of helium inlet flow rate

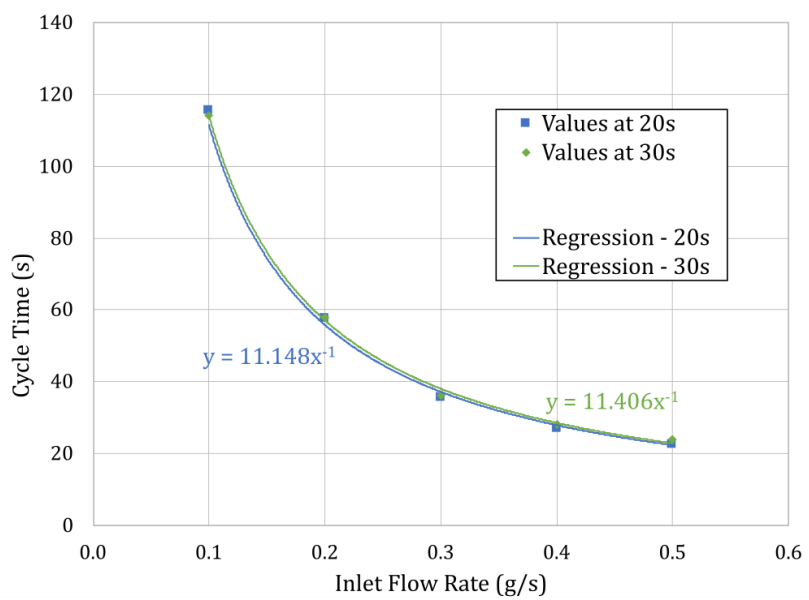


Figure 8. τ trend as a function of helium inlet flow rate, with evidence of proportionality

additional analysis performed on the variation of the characteristic time with respect to the helium flow rate entering the domain puts in evidence an inversely proportional trend, which translates in a linear dependence of the efficiency of removal from the inlet condition.

Table I. Values of τ at different times for increasing helium inlet flow rate, with evidence of proportional behavior

Helium inlet flow rate (g/s)	τ at 20 s (s)	Ratio (-)	τ at 30 s (s)	Ratio (-)
0.1	115.5280	1.000	114.1898	1.000
0.2	57.4712	0.497	57.7598	0.506
0.3	35.4788	0.307	36.1896	0.317
0.4	26.9033	0.233	28.0355	0.245
0.5	22.5792	0.195	23.9782	0.210

The results presented in this work constitute a step forward in the design and testing of the MSFR and help to lay the ground for further developments on the study of the helium bubbling system in particular. Additional studies can be now performed, as an example, with the definition of multiple gaseous species, in order to evaluate correctly the source term and the inventory of material going to the off-gas system, or with the usage of different correlations, with a proper sensitivity analysis. Additionally, the modelling of the behavior of metallic particles can be introduced as well, to investigate how the helium bubbling system would affect their removal as well.

RESEARCH DATA

The data that support the findings of this study are openly available in Zenodo at [<http://doi.org/10.5281/zenodo.4912612>].

FUNDING

This project has received funding from the Euratom research and training programme 2014-2018 under grant agreement no. 847527.

DISCLAIMER

The content of this paper does not reflect the official opinion of the European Union. Responsibility for the information and/or views expressed therein lies entirely with the authors.

REFERENCES

1. GIF, “Generation IV International Forum 2016 Annual Report,” (2016)
2. D. Gerardin et al., “Design evolutions of Molten Salt Fast Reactor,” *Proc. International conference on Fast Reactors and Related Fuel Cycles: Next Generation Nuclear Systems for Sustainable Development, Yekaterinburg, Russia, June 26-29*, (2017)

3. S. Delpech et al., "Reactor physic and reprocessing scheme for innovative molten salt reactor system," *Journal of Fluorine Chemistry*, **130** (1), pp. 11–17 (2009)
4. E. Cervi, S. Lorenzi, A. Cammi, and L. Luzzi, "Development of a multiphysics model for the study of fuel compressibility effects in the Molten Salt Fast Reactor," *Chemical Engineering Science*, **193**, pp. 379–393 (2019)
5. M. Aufiero et al., "An extended version of the SERPENT-2 code to investigate fuel burn-up and core material evolution of the Molten Salt Fast Reactor," *Journal of Nuclear Materials*, **441** (1-3), pp. 473–486 (2013)
6. E. Cervi, S. Lorenzi, A. Cammi, and L. Luzzi, "A multi-physics modelling approach for the evaluation of the gas bubbling system in the Molten Salt Fast Reactor," *Proc. 17th International Topical Meeting on Nuclear Reactor Thermal Hydraulics*, (2017)
7. M. Rhodes, *Introduction to Particle Technology: Second Edition*, John Wiley & Sons, Ltd, Chichester, UK (2008)
8. R. Higbie, "The rate of absorption of a pure gas into still liquid during short periods of exposure," *Institution of Chemical Engineers*, **35**, pp. 36–60 (1935)
9. G. Vijaya Kumar, M. Kampili, S. Kelm, K. Prakash, and H. Allelein, "Development and verification of a multi-species gas transport solver," *Proc. of the 14th OpenFOAM Workshop, Duisburg, Germany, 23–26 July 2019*, (2019)
10. H. Bonart, "Implementation and Validation of a Solver for Direct Numerical Simulations of Turbulent Reacting Flows in OpenFOAM," *Bachelor Thesis* (2012)
11. J. Leppänen, M. Pusa, T. Viitanen, V. Valtavirta, and T. Kaltiaisenaho, "The Serpent Monte Carlo code: Status, development and applications in 2013," *Annals of Nuclear Energy*, **82**, pp. 142–150 (2015)
12. A. Santamarina, D. Bernard, Y. Rugama, and OECD Nuclear Energy Agency., "The JEFF-3.1.1 nuclear data library : JEFF report 22, validation results from JEF-2.2 to JEFF-3.1.1," *OECD 2009 NEA No. 6807* (2009)
13. M. Brovchenko et al., "Neutronic benchmark of the molten salt fast reactor in the frame of the EVOL and MARS collaborative projects," *EPJ Nuclear Sciences & Technologies*, **5**, pp. 2 (2019)
14. M. Aufiero et al., "An extended version of the SERPENT-2 code to investigate fuel burn-up and core material evolution of the Molten Salt Fast Reactor," *Journal of Nuclear Materials*, **441**, pp. 473–486 (2013)
15. H. Rusche, "Computational Fluid Dynamics of Dispersed Two-Phase Flows at High Phase Fractions," *PhD thesis* (2002)
16. L. Schiller and A. Naumann, "Über die grundlegenden Berechnungen bei der Schwerkraftaufbereitung," *Verein Deutscher Ingenieure*, **44**, pp. 318–320 (1933)
17. W. E. Ranz and W. R. Marshall, "Evaporation from drops. Parts I & II.," *Chem. Eng. Progr*, **48**, pp. 141–173 (1952)
18. E. Cervi, "An Innovative Multiphysics Modelling Approach for the Analysis and the Development of the Generation IV Molten Salt Fast Reactor," *PhD thesis* (2020)